Presented at the 24th European PV Solar Energy Conference and Exhibition, 21-25 September 2009, Hamburg, Germany

MICRO-LUMINESCENCE SPECTROSCOPY ON MULTICRYSTALLINE SILICON

Paul Gundel[1*], Martin C. Schubert[1], Wolfram Kwapil[1], Jonas Schön[2], Manfred Reiche[3], Hele Savin[4], Marko Yli-Koski[4], Juan Angel Sans[5], Gema Martinez-Criado[5], Wilhelm Warta[1] and Eicke R. Weber[1]

[1]Fraunhofer Institute for Solar Energy Systems (ISE), Heidenhofstr. 2, 79110 Freiburg, Germany
[2]Freiburg Materials Research Center, University of Freiburg, Stefan-Meier-Str. 21, 79104 Freiburg, Germany
[3]Max Planck Institute for Microstructure Physics, Weinberg 2, 06120 Halle, Germany
[4]Helsinki University of Technology, P. O. Box 3500, 02015 TKK, Finland
[5]ESRF, 6 rue Jules Horowitz, BP 220, F-38043 Grenoble Cedex, France
[1*]paul.gundel@ise.fraunhofer.de

ABSTRACT: The luminescence of silicon has been used for many applications such as lifetime measurements and defect characterization in multicrystalline silicon for solar cells. In this paper we demonstrate new applications of luminescence spectroscopy for the characterization of multicrystalline silicon which are based on a very high spatial resolution in the order of one µm. These applications are the detection of small metal precipitates, the qualitative measurement of internal stress and X-ray Excited Optical Luminescence for correlating of X-ray fluorescence measurements with the minority carrier diffusion length.

Keywords: Photoluminescence, multicrystalline silicon, synchrotron, stress, precipitates

1 INTRODUCTION

Metal precipitates and internal stress are important to the processing and the performance of multicrystalline (mc) silicon solar cells. The precipitation of metals is relevant for mc silicon solar cells in many ways: Metal precipitation at crystal defects during the crystal growth can clean grains from impurities and thus, improve the performance [1], or can cause shunts and sites of pre-breakdown and damage the cell or module respectively [2,3]. These effects make the development of an accessible, fast and non-destructive technique for the detection of metal precipitates highly relevant for the further improvement of mc silicon solar cells. While at least the interstitial iron concentration is detectable with minority carrier lifetime measurement techniques [1,4] so far, the detection of single metal precipitates is only possible with technically demanding methods such as X-Ray Fluorescence spectroscopy (XRF) [5] or Transmission Electron Microscopy (TEM), which requires a time-consuming sample preparation and pre-characterisation [4].

Internal stress can, as well as metal precipitates, significantly reduce the quality of mc silicon solar cells. Internal stress reduces the mechanical stability of silicon wafers. Furthermore stress is known to amplify the formation of dislocations and influence the distribution of impurities. Since dislocations and impurities limit the efficiency potential in mc silicon solar cells, a deeper knowledge about stress related defects has high significance for photovoltaics. Stress in mc silicon was recently measured by micro-Raman spectroscopy by Becker et al. [6]. They demonstrated a sophisticated method to measure stress tensors and showed examples for the correlation between dislocation clusters and stress.

In this paper we demonstrate photoluminescence (PL) based techniques to detect micron or even smaller sized metal precipitates and to qualitatively measure internal stress. The results are confirmed by XRF measurements at the beamline ID22 of the European Synchrotron Radiation Facility (ESRF) and by Raman measurements, respectively. The detection of metal precipitates is based on the recombination activity of precipitates which in turn reduces the band-to-band PL. In contrast, the stress measurement is based on the stress-induced shift of the bandgap energy, which also shifts the band-to-band PL peak. These PL based techniques offer the advantage to correlate internal stress and the position of precipitates directly without any spatial ambiguity to other material parameters such as minority carrier lifetime and defect luminescence.

Furthermore we demonstrate luminescence spectroscopy to be a highly suitable technique for correlating data from synchrotron-based measurements with other material parameters. So far only X-ray Beam Induced Current (XBIC) [7] has been available for identifying regions of low minority carrier lifetime, analyzing the recombination activity of metal precipitates and correlating metal precipitate-rich areas with other material parameters in-situ. XBIC requires the preparation of Schottky contacts, which have the potential to increase the background noise for XRF due to additional scattering. Furthermore each preparation step increases the risk to unintentionally contaminate the sample and thus invalidating experimental data.

Therefore, a contactless in-situ measurement technique of the minority carrier lifetime is highly desirable. We present X-ray Excited Optical Luminescence (XEOL) as suitable method. For this we measured the XEOL of crystalline silicon and compared a line scan acquisition of the XEOL band-to-band intensity to the positions of grain boundaries and the copper Kα peak intensity of a XRF scan, which was measured simultaneously. In recent publications [8,9] XEOL was applied to samples with high luminescence efficiency such as direct bandgap semiconductors and porous silicon. Crystalline silicon, having an indirect

bandgap, has a significantly lower [10] luminescence efficiency and requires a high x-ray flux and a very sensitive luminescence detection system. The XEOL and the XRF measurements were carried out at ESRF on beamline ID22.

2 EXPERIMENTAL

2.1 Photoluminescence setup

The PL spectroscopy setup is a confocal microscope with an excitation laser (532 nm wavelength) with a power of 10 mW on the sample. The PL light is split up by a 150 g mm^{-1} grating and detected by an InGaAs detector. For these experiments a 50x lens with a resulting depth of focus of 3 µm is used. This confocal setup provides a radial resolution of about 0.8 µm and a spectral resolution of 0.5 nm.

2.2 Detection of metal precipitates

The detection of metal precipitates is demonstrated on Direct Bonded Wafers (DBW), which were intentionally contaminated with iron or copper. More details on the preparation of DBWS can be found in [11]. The DBWs were contaminated either with iron or with copper by indiffusion at 1030 °C and 1200 °C respectively. In addition, a reference DBW was subject to the same heat treatment without any contamination. For the analysis of cross contamination effects one DBW was contaminated with iron and copper with the same heat treatment as for the iron contamination. More details on the contamination are available in [12]. Finally the DBWs were prepared with a bevelled polish and a subsequent surface cleaning etch in order to allow PL measurements at the dislocation network at the interface between the two bonded wafers.

2.3 Stress measurements

The confocal PL setup with its spatial and spectral resolution is suitable as well for the qualitative measurement of internal stress. The stress dependence of the bandgap energy was first reported in 1958 for hydrostatic stress [13] and in 1962 for uniaxial stress [14]. These experimental results were theoretically confirmed [15, 16].

For uniaxial stress σ the bandgap energy does not only depend on the absolute stress value but also slightly on the stress direction in respect to the crystal orientation. Due to a split up of the X_1 and an energy shift of the X_1 and the $\Gamma_{25'}$ levels at uniaxial stress σ the minimum indirect bandgap energy $E_{\Gamma\text{-}X(min)}$, which is determining the radiative recombination rate, is

$$E_{\Gamma-X} = E_0 - \alpha \ *10^{-3} * \frac{meV}{MPa} * \sigma \qquad (1)$$

with α being 108.3 (for uniaxial stress in the [100] direction), 109 ([111] direction) and 102 ([110] direction), respectively, as theoretically determined in [16]. With changing bandgap energy also the peak of the band-to-band luminescence is shifted. This effect was shown to be in good agreement with theoretical values at 4.2 K for uniaxial stress [17] and at room temperature for hydrostatic stress [18] in monocrystalline silicon wafers.

In this paper we utilize this shift of the band-to-band photoluminescence (PL) for the determination of the stress distribution in multicrystalline silicon.

PL measurements can provide a scalar for stress but are unable to represent the tensor properties of stress, due to the fact, that no polarisation dependence of the band-to-band PL was reported in [19] and also could not be detected in this work. Therefore, we make the simplifying assumption of uniaxial stress and an average α in (1) of 106.4. More details on these simplifications can be found in [20].

These assumptions allow calculating the stress with equation (1) from the band-to-band PL shift. We call this method Stress Mapping by Photoluminescence Spectroscopy (SMAPS).

SMAPS offers the advantage of providing complementary material parameters within the same measurement with precise local alignment. By integrating the band-to-band peak a qualitative measure for the minority carrier lifetime τ can be extracted, since the intensity of the band-to-band peak is proportional to τ^2 [21] in the high injection level. Furthermore dislocation PL can be detected and gives additional information about the minority carrier lifetime limiting defects [19, 22].

2.4 X-ray Excited Optical luminescence

The setup is as follows: The pink beam ($\Delta E/E \simeq 10^{-2}$) is focused by a Kirkpatrick mirror system on a spot of approximately 1 µm in diameter on the sample with a flux of about 10^{12} s^{-1} at 17.5 keV. The XRF is collected by a Si drift detector and the XEOL by an aspheric lens coupled via multi-mode fiber optics (50µm core) to a monochromator (f/4, 101 mm focal length) equipped with an InGaAs multi-channel diode detector (512 pixel elements; 14 x 200 μm^2 pixel size) compatible for fast and easy computer interfacing. More details on this XEOL setup can be found in [23,24]. All measurements are carried out at room temperature.

The intensity of the optical luminescence is determined by the minority carrier density [3]. Each absorbed x-ray photon excites on average one electron-hole pair for each 3.6 eV of energy. The absorption length in silicon for x-rays at 17.5 keV is 625 µm.

The samples used here are a 10^{16} cm^{-3} boron doped floatzone sample with an effective minority carrier lifetime of 600 µs, and a mc silicon 10^{16} cm^{-3} boron doped sample intentionally contaminated with transition metals. The average minority carrier lifetime of the latter sample is 5 µs, which is quite low for solar grade mc silicon. Since synchrotron-based research on mc silicon is often carried out on intentionally contaminated wafers, the feasibility of XEOL on low lifetime wafers is of high relevance for further applications.

3 RESULTS AND DISCUSSION

3.1 Detection of metal precipitates

In the iron contaminated sample the intensity of the band-to-band PL peak is reduced at the dislocation network (which intersects the surface of the bevelled sample to the right side of the blue line in Fig. 1) due to its recombination activity. At some distinct spots of a size between 1 µm and 4 µm the band-to-band PL peak is particularly low (circles in Fig. 1 (a)). At these spots iron precipitates were detected by XRF (Fig. 1 (b)). Both measurements show a good agreement which

demonstrates the potential of micro-PL spectroscopy to detect precipitates due to their increased recombination activity. The agreement is especially remarkable, since the escape depth (the depth from which luminescence reaches the sample surface) of the PL is smaller than the information depth of the fluorescence. As expected, XRF did not detect any impurities other than iron in this sample.

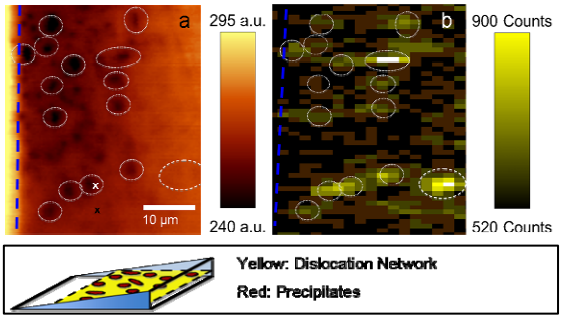

Figure 1: Below: Scheme of the sample preparation with the bevelled polish. Above: Intensity of the band-to-band PL peak at room temperature (a) and of the iron x-ray Kα fluorescence (b). The dislocation network intersects the surface to the right of the dashed blue line. The spots with reduced band-to-band PL intensity (white circles) are caused by recombination active precipitates, which were detected with XRF (b). The PL measurement clearly shows more details than the XRF measurement, which suggests a higher sensitivity and spatial resolution.

The dashed circle shows a limitation of the micro-PL setup. The sensitivity is limited to an area close to the surface because of the short absorption length of the excitation laser (about 1µm). Since the iron precipitate in the dashed circle lays deeper in the sample, it cannot be detected by the current micro-PL setup. This limitation might be overcome by an excitation laser with a longer wavelength and absorption length in silicon.

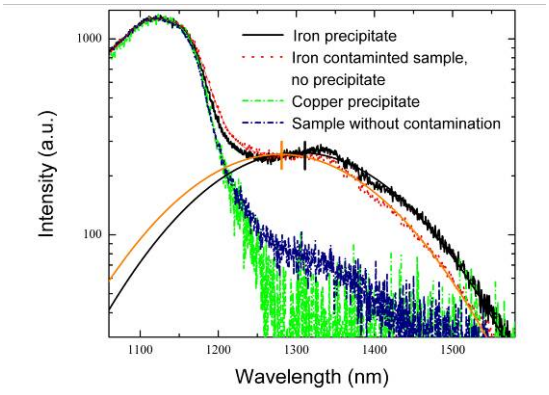

Figure 2: Comparison of the normalised room temperature PL spectra at an iron precipitate (white x in Fig. 1), at a position without precipitate (black x in Fig. 1), the bonded wafer without contamination and at a copper precipitate (white x in Fig. 1). The defect PL at the iron precipitate is shifted to longer wavelengths, which can be seen from the fit of the defect PL (thin orange curve – no precipitate, thin black curve – precipitate) with the thick vertical lines marking the peak positions. The band-to-band peak is also fitted, but the fit function is not shown for the sake of clarity.

The iron precipitates alter not only the band-to-band PL but also the defect PL. In Fig. 2 four normalised PL spectra are compared: (1) At an iron precipitate (white x in Fig. 1), (2) at a position without precipitate (black x in Fig. 1), (3) the reference DBW, which was subject to the same temperature steps as the iron contaminated sample, without contamination and (4) at a copper precipitate.

The iron contaminated sample shows an enhanced defect PL at 1.3 µm compared to the uncontaminated sample, when the spectra are normalized to the band-to-band PL. The spectra are multiplied by the factors: 1 for the iron precipitate, 0.72 for the iron contaminated sample at no precipitate, 7.8 for the copper precipitate and 0.74 for the uncontaminated sample. In the copper contaminated sample the defect PL is drastically reduced.

At the iron precipitate the broad defect PL band is shifted to longer wavelengths. If this is due to an additional peak with a longer wavelength, which is suggested by the decreased quality of the fit for the defect PL with one Gauss peak (see Fig. 2), or due to an energy shift of the peak cannot be conclusively decided from these data. The defect PL is weaker in the uncontaminated sample.

A comparison between the intensity of the band-to-band PL and XRF measurements of the copper contaminated sample as well as more details on the energy shift of the defect PL are shown in [12].

3.2 SMAPS

The best results for detecting the stress induced spectral shift were achieved by empirically fitting the band-to-band PL with three overlapping Gaussian peaks, which have fixed amplitude ratios, fixed spectral distances and fixed spectral widths. In addition a defect luminescence peak at 1250 nm (fixed position and spectral width) is included in the fit (see Fig. 5). This fitting routine results in three fitting parameters: (i) the amplitude, which is a measure for the minority carrier lifetime, and (ii) the spectral position, which is a measure for stress, of the band-to-band peak and (iii) the amplitude of the defect peak at 1250 nm. In this way a relative shift of the band-to-band PL peak can be determined.

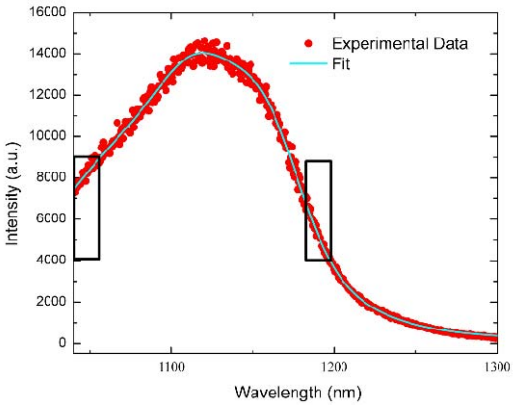

Figure 3: Example for the fit with three Gauss peaks for the band-to-band PL with fixed amplitude ratios, fixed spectral distances and fixed spectral widths and an additional peak at 1240 nm for the dislocation luminescence. The rectangles denote the details, which are shown in Fig. 4.

A representative example for the fitting curve is shown in Fig. 3. The minority carrier lifetime does not influence the centre of the peak, since the PL intensity depends in the same way on τ for any wavelength of the band-to-band peak, if reabsorption is neglected. More details on this fitting procedure and the resulting uncertainties are stated in [20].

From the energy shift of the band-to-band PL the stress levels can be calculated with equation (1). Details of a spectrum at tensile and of a spectrum at compressive stress are shown in Fig. 4, which demonstrates the relative spectral shift of the peak.

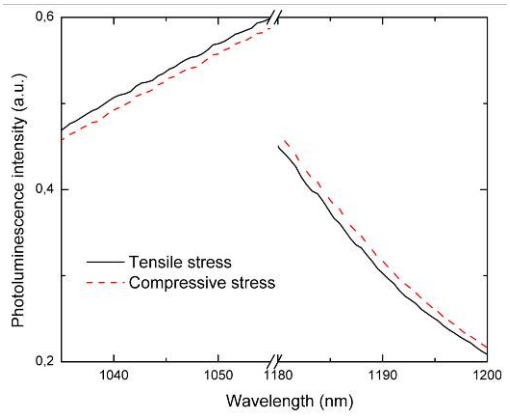

Figure 4 Details of two normalized spectra for an area with compressive and an area with tensile stress are shown to demonstrate the relative shift of the spectra. The lines are moving averages over 5 points for an easier comparison. The positions of these details are marked in Fig. 3.

For the evaluation of SMAPS we measured the spatially resolved PL spectra of a standard industrial mc silicon wafer from the middle of an ingot. This 10^{16} cm^{-3} boron doped wafer was polished and the surface was left unpassivated. Due to the resulting high surface recombination velocity of about 10^5 cm s^{-1} [25] the effective τ is limited to 5 µs. Therefore the PL intensity, which is proportional to τ^2, is rather small. An integration time of 4 s per pixel was sufficient to get an image of the frequency shift (see Fig. 5 on the left). For the PL spectroscopy 3 pixels were measured for each 2 µm. For the Raman spectroscopy 2 pixels per µm were measured with an integration time of 0.07 s for each pixel. The details on the Raman measurement can be found in [20]. In Fig. 5 SMAPS is compared to the stress, which is calculated from the Raman measurement without a specific orientation setting. The average of all pixels is taken as 0-stress level in all cases.

This comparison reveals that both measurements are in good qualitative agreement. But the stress is by a factor 7 higher for the Raman results. A detailed analysis of this deviation including measurements with different spatial resolutions and at 77 K is given in [20]. From this analysis we conclude that the deviation is due to either defect luminescence close to the band-to-band PL or the broadness of the band-to-band PL peak and the resulting noise at 300 K in the shift determination is reducing the detectable shift and thus the calculated stress at room temperature.

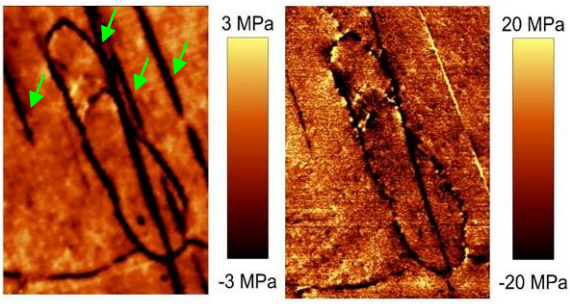

Figure 5 The comparison of the stress calculated from a PL measurement on the left side and the stress calculated from a Raman measurement on the right side shows qualitative agreement between both measurements. The straight lines are scratches from the polishing on the front side (arrows). The Raman determined stress is by a factor 7 higher than the PL determined stress.

The SMAPS and Raman maps in Fig. 5 suggest that this effect decreases the calculated absolute stress systematically. For a possible empirical correction of this effect by multiplying the result with a constant factor a broader experimental basis is required.

3.3 XEOL

In order to analyze the optical system at ID22 for the detection of silicon luminescence the high minority carrier lifetime floatzone sample with the consequently high band-to-band PL in comparison to mc silicon was used. A spectrum of the luminescence was recorded by measuring 40 overlapping spectra (each spectrum covers a bandwidth of 70 nm) in the range between 870 nm and 1280 nm. The integration time for each spectrum was 150 s. The stitched spectra show a clear peak at 1130 nm (see Fig. 6), which is characteristic for crystalline silicon at room temperature. The comparison with the simulated spectrum reveals that the peak position is in good agreement with the theoretical expectation, but the width is decreased. The small peaks (e.g. at 1200 nm) with their homogenous distance of 20 nm are most likely due to a Fabry-Perot effect within the sample. This assumption is suggested by their decreasing intensity with increasing spectral distance from the band-to-band peak and their fixed spectral distance. The Fabry-Perot effect could also be responsible for the decreased width of the band-to-band peak.

To check the feasibility of XEOL on low minority carrier lifetime silicon, a XEOL spectrum of the mc silicon sample was recorded. The peak around 1130 nm is clearly visible, which is in good agreement with the theoretical curve. The details on this spectrum and its deviations from the theoretical curve are analyzed in [24].

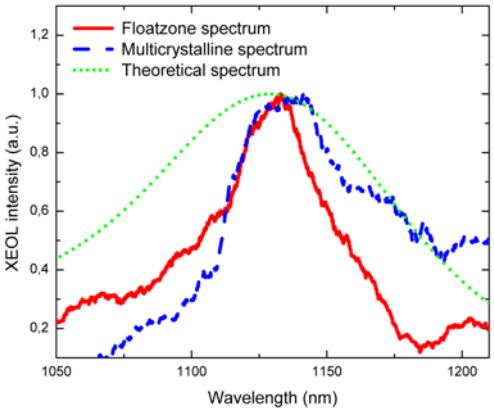

Figure 6 XEOL spectrum of floatzone silicon, spectrum of a mc silicon sample and theoretically calculated curve. The peak positions of both spectra agree well with the theoretical curve, but the width is smaller than in theory. In addition some secondary maxima are visible. The background seems to increase for longer wavelengths for the mc silicon.

In Figs. 7 and 8 a possible application for XEOL measurements is exemplified. In order to correlate XRF data with additional material parameters, XEOL is used in-situ to locate recombination active areas such as grain boundaries, which can in turn be easily located with ex-situ minority carrier lifetime measurement methods. For illustration a line scan of the XEOL intensity and the XRF spectrum are simultaneously measured. Since the diffusion length of the minority carriers limits the spatial resolution, a step width of 15 µm was chosen for this line scan. Fig. 7 shows the line scan of the XEOL intensity (integrated between 1085 nm and 1155 nm), which is embedded into the optical microscope image of the according area. The integration time for the mc sample was 400 s for each pixel. Fig. 7 shows, that the XEOL intensity is decreased at the grain boundaries visible in the microscope image (white arrows).

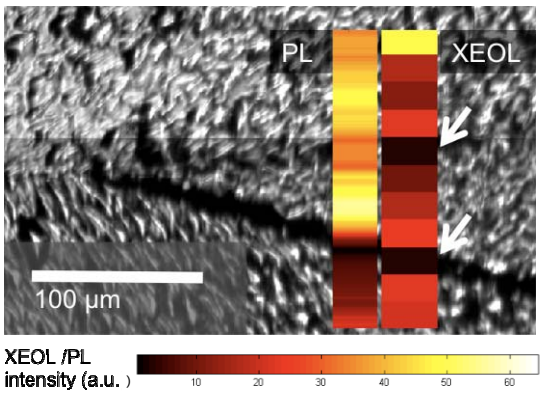

Figure 7 Line scan of the XEOL intensity (right) integrated between 1085 nm and 1055 nm wavelength and a PL line scan (left) embedded into a light microscope image. The XEOL intensity is decreased at the recombination active grain boundaries (white arrows). The comparison to the line scan of the band-to-band PL (integrated between 1050 nm and 1200 nm) on the left side shows a reasonable agreement between both measurements.

The comparison between the XEOL line scan and the band-to-band PL map (Fig. 7) shows a reasonable agreement between both measurements. Deviations between both measurements could be caused by the different depths of information of both techniques, which are up to 5µm for the PL and up to the wafer thickness for XEOL. The visible light microscope was aligned to the x-ray microbeam by measuring the position of a gold knife-edge, which results in a precision of about 2 µm.

In Fig. 8 the line scan of the XRF intensity of the copper Kα line is depicted. The XRF spectra were simultaneously gathered with the XEOL measurements in Fig. 7. The scan shows that at the upper grain boundary the copper intensity is increased. The decreased XEOL intensity and the increased Cu XRF intensity at this grain boundary were confirmed by an additional measurement.

Figs. 7 and 8 show that a correlation between XEOL and XRF is possible, even if the alignment between microscope image and XRF is not as precise as in this example or the recombination defects are not visible with a light microscope, which is usually the case for small angle grain boundaries and dislocations.

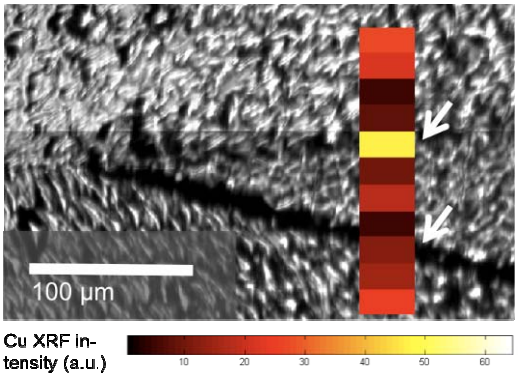

Figure 8 Line scan of the XRF intensity of the copper Kα line embedded into a light microscope image. The copper concentration at the upper grain boundary (white arrow) is increased.

4 CONCLUSION

In this paper we demonstrated the broad range of applicability of micro-luminescence spectroscopy. On contaminated direct bonded wafers we were able to detect metal precipitates with a size of 1 µm or below by a confocal photoluminescence (PL) spectroscopy setup and could observe an element specific effect of the precipitates on the defect luminescence.

With the same setup a qualitative stress measurement technique based on the stress induced bandgap energy shift was developed. This stress measurement technique was evaluated by Raman measurements. The new technique, which we call SMAPS, offers the advantage to allow directly correlating internal stress to other material parameters such as the minority carrier lifetime and defect luminescence.

For synchrotron-based research on multicrystalline silicon X-ray Excited Optical Luminescence (XEOL) was introduced as a new technique complementary to XBIC. A XEOL line scan acquisition is compared to a PL and an X-Ray Fluorescence (XRF) spectroscopy scan,

which demonstrate the applicability of XEOL to distinguish electrically good and bad areas and to correlate x-ray fluorescence measurements to the recombination activity in-situ.

5 ACKNOWLEDGEMENT

We gratefully acknowledge N. Bayer, M. Hecht, T. Kalden, M. Kwiatkowska, H. Lautenschlager, R. Neubauer and G. Räuber for sample preparation. We acknowledge the European Synchrotron Radiation Facility for provision of synchrotron radiation facilities at ID22. This work was partly funded by the project Silicon Beacon and is financially supported by the German Federal Ministry for the Environment, Nature Conservation and Nuclear Safety within the research cluster SolarFocus (0327650) and all the industry partners.

References

[1] J. Bailey and E. R. Weber, Phys. Stat. Sol. A **137**, 515 (1993).
[2] V. Hoffmann, K. Petter, J. Djordjevic-Reiss et al., in Proc. of 23rd EU-PVSEC, Valencia, (2008).
[3] J. Isenberg, W. Warta, J.Appl. Phys. 95, 5200 (2004).
[4] S. Sadamitsu, A. Sasaki, M. Hourai, S. Sumita and N. Fujino, Jpn. J. Appl. Phys. **30,** 1591 (1991).
[5] T. Buonassisi, M. Heuer, A.A. Istratov, M.D. Pickett, M.A. Marcus, E.R. Weber, Acta Materialia **55**, 6119 (2007).
[6] M. Becker, H. Scheel, S. Christiansen, and H. P. Strunk, J. Appl. Phys. **101**, 063531 (2007).
[7] T. Buonassisi, A.A. Istratov, M.D. Pickett, M.A. Marcus, G. Hahn, S. Riepe, J. Isenberg, W. Warta, G. Willeke, T.F. Ciszek, and E.R. Weber, Appl. Phys. Lett. **87**, (2005).
[8] T.K. Sham, R. Sammynaiken, Y.J. Zhu, P. Zhang, I. Coulthard and S.J. Naftel, Thin Solid Films **363**, (2000).
[9] G. Martinez-Criado, B. Alen, A. Homs, A. Somogyi, C. Miskys, J. Susini, J. Pereira-Lachataignerais, and J. Martinez-Pastor, Appl. Phys. Lett. **89**, 221913 (2006).
[10] T. Trupke, J. Zhao, A. Wang, R. Corkish, and M.A. Green, Appl. Phys. Lett. 82, 2996 (2003).
[11] M. Kittler, X. Yu, O.F. Vyvenko, M. Birkholz, W. Seifert, M. Reiche, T. Wilhelm, T. Arguirov, A. Wolff, W. Fritzsche, M. Seibt, Materials Science and Engineering: C **26**, 5-7 (2006).
[12] P. Gundel, M.C. Schubert, W. Kwapil, J. Schön, M. Reiche, H. Savin, M. Yli-Koski, J.A. Sans, G. Martinez-Criado, W. Seifert, W. Warta and E.R. Weber, Phys. Stat. Sol. RRL **3**, 230 (2009).
[13] W. Paul and D. M. Warschauer, J. Phys. Chem. Sol. **5**, 89 (1958)
[14] W. Rindner, J. Appl. Phys. **33**, 2479 (1962).
[15] I. Goroff, and L. Kleinman, Phys. Rev. **132**, 1080 - 1084 (1963).
[16] J. J. Wortman, J. R. Hauser, and R. M. Burger, J. Appl. Phys. **35**, 7, 2122 (1964).
[17] K. Yasutake, M. Umeno, H. Kawabe, H. Nakayama, T. Nishino, and Y. Hamakawa, Jpn. J. Appl. Phys. **21**, 12, 1715 (1982).
[18] Y. Ishibashi, T. Kobayashi, A. D. Prins, J. Nakahara, M. A. Lourenco, R. M. Gwilliam, K. P. Homewood, Phys. Stat. Sol (b) **244**, 1, 402 (2007).
[19] S. Ostapenko, I Tarasov, J P Kalejs, C Haessler and E-U Reisner Semicond. Sci. Technol. **15**, 840, (2000).
[20] P. Gundel, M. C. Schubert, W. Warta, Phys. Stat. Sol. A. (2009), submitted.
[21] P. Würfel, J. Phys. C 15, 3967 (1982.)
[22] M. Suezawa and K. Sumino, Phys. Stat. Sol. A **78** (1983).
[23] G. Martinez-Criado, R. Steinmann, B. Alen, A. Labrador, D. Fuster, J. M. Ripalda, A. Homs, S. Laboure, and J. Susini, Rev. Sci. Instrum. **78**, 025106 (2007).
[24] P. Gundel, G. Martinez-Criado, M. C. Schubert, J. A. Sans, W. Kwapil, W. Warta and E. R. Weber, Phys. Stat. Sol. RRL **3**, No. 7, 275– 277, (2009).
[25] A.A. Istratov, H. Hieslmair, and E. R. Weber, Appl. Phys. A: Mater. Sci. Process. **A70**, 489 (2000).